# Engineering Calculations of Three-Dimensional Inviscid Hypersonic Flowfields

Christopher J. Riley*
*NASA Langley Research Center, Hampton, Virginia 23665*
and
Fred R. DeJarnette†
*North Carolina State University, Raleigh, North Carolina 27695*

**An approximate solution technique has been developed for three-dimensional, inviscid, hypersonic flows. The method uses Maslen's explicit pressure equation and the assumption of approximate stream surfaces in the shock layer. This approximation represents a simplification of Maslen's asymmetric method. The solution procedure involves iteratively changing the shock shape in the subsonic-transonic region until the correct body shape is obtained. Beyond this region, the shock surface is determined by using a marching procedure. Results are presented for a paraboloid and elliptic cone at angle of attack. Calculated surface pressure distributions, shock shapes, and property profiles are compared with experimental data and finite difference solutions of the Euler equations. Comparisons of the results of the present method with experimental data and detailed predictions are very good. Since the present method provides a very rapid computational procedure, it can be used for parametric or preliminary design applications. One useful application would be to incorporate a heating procedure for aerothermal studies.**

## Nomenclature

$B,b,c,d$ = conic section parameters
$\hat{e}_x,\hat{e}_r,\hat{e}_\phi$ = unit vectors of cylindrical coordinate system
$\hat{e}_\xi,\hat{e}_\beta,\hat{e}_n$ = unit vectors of curvilinear coordinate system
$f$ = shock radius, nondimensionalized by $L$
$H$ = total enthalpy, nondimensionalized by $V_\infty^2$
$h$ = static enthalpy, nondimensionalized by $V_\infty^2$
$h_\xi,h_\beta,h_n$ = scale factors of curvilinear coordinate system, nondimensionalized by $L$
$K$ = shock curvature, nondimensionalized by $1/L$
$L$ = reference length
$M$ = Mach number
$p$ = static pressure, nondimensionalized by $\rho_\infty V_\infty^2$
$\dot{q}$ = heat transfer rate
$R$ = radius of curvature, nondimensionalized by $L$
$s$ = surface distance, nondimensionalized by $L$
$u,v,w$ = velocity components of curvilinear coordinate system, nondimensionalized by $V_\infty$
$V$ = velocity magnitude
$\mathbf{V}$ = velocity vector, nondimensionalized by $V_\infty$
$x,r,\phi$ = cylindrical coordinate system, nondimensionalized by $L$
$x,y,z$ = Cartesian coordinate system, nondimensionalized by $L$
$\alpha$ = angle of attack
$\Gamma$ = shock wave angle relative to freestream velocity
$\gamma$ = ratio of specific heats
$\delta_\phi$ = shock wave angle in circumferential direction
$\epsilon$ = axial distance from origin at which integration of shock variables is started
$\theta$ = inclination angle of body
$\xi,\beta,\eta$ = curvilinear coordinate system, nondimensionalized by $L$
$\rho$ = density, nondimensionalized by $\rho_\infty$
$\sigma$ = shock wave angle, $\phi - \delta_\phi$
$\Phi,\psi$ = stream functions, nondimensionalized by $\rho_\infty V_\infty L^2$

*Subscripts*

$b$ = value on body
$c$ = property on conical afterbody
$i$ = conic section parameters specific to $\phi$ = const plane
$j$ = marching step
ref = reference value
$s$ = value on shock surface
$w$ = wall value
$\infty$ = freestream conditions

Presented as Paper 91-0701 at the AIAA 29th Aerospace Sciences Meeting, Reno, NV, Jan. 7-10, 1991; received Feb. 15, 1991; revision received May 23, 1991; accepted for publication May 28, 1991. 

*Aerospace Technologist, Aerothermodynamics Branch, Space Systems Division, M.S. 366. Member AIAA.

†Professor, Mechanical and Aerospace Engineering Department, Box 7910. Associate Fellow AIAA.

## Introduction

An approximate solution to the three-dimensional inviscid, hypersonic flowfield equations could be an important element in the multidisciplinary design of aerospace vehicles. The results of the inviscid analysis influence the aerodynamic, performance, and control issues involved in the design of the vehicle. Additionally, the inviscid results could serve as inputs for the prediction of vehicle heat loads during the preliminary thermal design process. Coupled inviscid-viscous calculations have been demonstrated previously to predict adequately the heating over a wide range of geometries and aerothermal environments.[1-3] The three-dimensional inviscid solutions used by these engineering aerodynamic heating methods differ in complexity from simple modified Newtonian theory[1] to more exact finite difference solutions of the three-dimensional Euler equations.[3,4] Modified Newtonian theory is simple to use, but its accuracy is limited. Numerical solutions of the inviscid equations[4-7] may be too computer intensive in a preliminary design study. A rapid but accurate approximate three-dimensional inviscid analysis would significantly enhance current engineering aerothermal capabilities.

Surface heating rates over re-entry vehicles have also been obtained by numerically solving the Navier-Stokes (NS) equations[8] and their various subsets including the parabolized Navier-Stokes[9] and viscous shock layer equations.[10,11] With continued increasing confidence in the application of the detailed NS codes, final design studies will eventually incorporate these methods. However, these methods presently require excessive computer storage and computer time to be practical in a preliminary design environment where a range of geometries and flow parameters are to be studied. An approximate three-dimensional inviscid method coupled with an engineering aerodynamic heating prediction method can easily be run on a computer workstation and complements the detailed computational fluid dynamic (CFD) methods in the design of re-entry vehicles.

Maslen[12] developed an approximate inviscid flowfield method for axisymmetric bodies using an explicit expression for the first-order pressure along lines normal to the shock wave. Since the body shape is determined from a given shock shape, this method is referred to as an inverse technique. Solving for a specified body shape can be accomplished indirectly by iteration of the shock shape.[13,14] This calculation gives reasonable results, except for flow recompression regions.

Maslen[15] subsequently outlined a method for three-dimensional inviscid flow and improved the explicit pressure equation by deriving a second-order approximation of the momentum equation normal to the shock. Although more accurate, the three-dimensional method is complicated and unwieldy. In fact, only preliminary results were presented for blunt-body flows.[16,17]

The present analysis simplifies the asymmetric problem of Maslen[15] by using two stream functions that approximate the actual stream surfaces in the shock layer and a modified form of the Maslen second-order pressure equation. Comparisons of the present results in terms of shock layer profiles, surface pressure distributions, and shock shapes are presented with Euler predictions and experimental data for a paraboloid and a blunted cone with an elliptical cross section at angle of attack in order to demonstrate the capability of the present approximate method.

## Analysis

### Coordinate System

For a three-dimensional shock wave, a cylindrical coordinate system $(x, r, \phi)$ is used, and the $x$ axis is aligned with the freestream velocity vector. The shock wave geometry[18] may be described by

$$r_s = f(x, \phi) \tag{1}$$

Two angles that define the shock wave shape are

$$\tan\delta_\phi = \frac{1}{f}\frac{\partial f}{\partial \phi} \tag{2}$$

$$\tan\Gamma = \frac{\partial f}{\partial x}\cos\delta_\phi \tag{3}$$

A third angle is given by the relation

$$\sigma = \phi - \delta_\phi \tag{4}$$

All three angles are shown in Fig. 1. For the special case of axisymmetric flow, $\Gamma = \Gamma(x)$, $\delta_\phi = 0$, and $\sigma = \phi$.

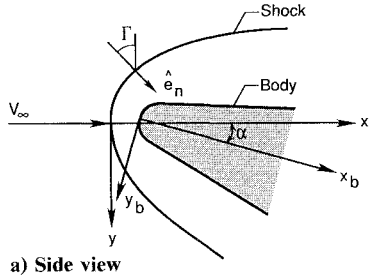

a) Side view

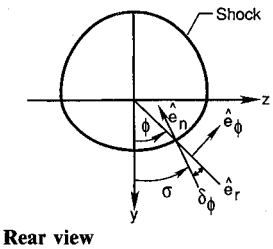

b) Rear view

**Fig. 1 Shock wave and body geometry.**

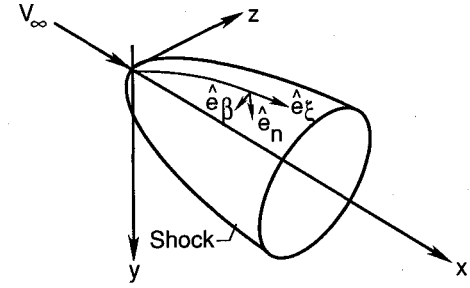


**Fig. 2 Shock-oriented curvilinear coordinate system.**

Next, a shock-oriented curvilinear coordinate system $(\xi,\beta,n)$ is defined with corresponding unit vectors $(\hat{e}_\xi,\hat{e}_\beta,\hat{e}_n)$ and velocities $(u,w,v)$. This coordinate system[1,19] is appropriate for hypersonic flow $(M_\infty \gg 1)$ and thin shock layers. The unit vector $\hat{e}_{ns}$ is the inward vector normal to the shock surface. The coordinates $\xi$ and $\beta$ are chosen such that $\hat{e}_{\xi s}$ is in the direction of the tangential velocity component just inside the shock surface. The unit vector $\hat{e}_{\beta s}$ is perpendicular to $\hat{e}_{\xi s}$ and $\hat{e}_{ns}$ (see Fig. 2). This coordinate system is defined as orthogonal at the shock surface but is nonorthogonal in the shock layer for a general three-dimensional shock.[19] However, the coordinate system may be assumed to be orthogonal for thin shock layers.

The postshock relations can be written as

$$V_s = u_s\hat{e}_{\xi s} + v_s\hat{e}_{ns} \tag{5a}$$

$$w_s = 0 \tag{5b}$$

whereas, in general, through the shock layer,

$$V = u\hat{e}_\xi + v\hat{e}_n + w\hat{e}_\beta \tag{6}$$

The component of the freestream velocity tangent to the shock wave is unchanged across the shock wave; therefore, the unit vectors $\hat{e}_\xi$, $\hat{e}_\beta$, and $\hat{e}_n$ at the shock are

$$\hat{e}_{\xi s} = \cos\Gamma\hat{e}_x + \sin\Gamma(\cos\delta_\phi\hat{e}_r - \sin\delta_\phi\hat{e}_\phi) \tag{7a}$$

$$\hat{e}_{\beta s} = \sin\delta_\phi\hat{e}_r + \cos\delta_\phi\hat{e}_\phi \tag{7b}$$

$$\hat{e}_{ns} = \sin\Gamma\hat{e}_x - \cos\Gamma(\cos\delta_\phi\hat{e}_r - \sin\delta_\phi\hat{e}_\phi) \tag{7c}$$

The differential arc lengths along each coordinate direction $(\xi, \beta, n)$ are $h_\xi\, d\xi$, $h_\beta\, d\beta$, and $h_n\, dn$, respectively. The scale factors $h_\xi$, $h_\beta$, and $h_n$ govern the stretching of the corresponding coordinates and are given by

$$h_\xi = h_{\xi s}(1 - nK_\xi) \tag{8a}$$

$$h_\beta = h_{\beta s}(1 - nK_\beta) \tag{8b}$$

$$h_n = 1 \tag{8c}$$

where $K_\xi$ and $K_\beta$ are the curvatures of the shock surface in the $\xi$-$n$ and $\beta$-$n$ planes, respectively. The curvatures may also be defined as

$$K_\xi = -\frac{1}{h_{\xi s}}\frac{\partial \Gamma}{\partial \xi} \tag{9}$$

$$K_\beta = \frac{\cos\Gamma}{h_{\beta s}}\frac{\partial \sigma}{\partial \beta} \tag{10}$$

**Governing Equations**

*Stream Functions*

The continuity equation for three-dimensional flows given by

$$\nabla \cdot (\rho V) = 0 \tag{11}$$

is satisfied by two stream functions. The continuity equation can be written as

$$\rho V = \nabla\psi \times \nabla\Phi \tag{12}$$

where $\psi$ and $\Phi$ represent the two stream functions.[15]

As noted in Refs. 12 and 15 for blunt bodies at hypersonic speeds, most of the mass flow is near the shock wave where the velocity component $w$ is small. A simplifying assumption is made in this study that $w = 0$ throughout the shock layer. This assumption is inaccurate near the body surface but has little effect on the shock shape and surface pressures. Thus, if $\Phi$ is set equal to $\beta$, $\psi$ becomes

$$\frac{\partial \psi}{\partial n} = -\rho u h_\beta \tag{13}$$

$$\frac{\partial \psi}{\partial \xi} = \rho v h_\xi h_\beta \tag{14}$$

These definitions of $\psi$ and $\Phi$ are not unique, and they satisfy the exact flowfield equations only at the shock wave. The intersections of $\beta$ = const planes with the shock surface are referred to as shock lines. Shock lines are in the direction of the $\xi$ coordinate, and for axisymmetric flow, $\beta$ = const planes are meridional planes.

*Pressure Equation*

The momentum equations for steady, inviscid flow may be written as

$$\rho(V \cdot \nabla V) + \nabla p = 0 \tag{15}$$

Writing these equations in the $\xi,\beta,n$ system gives the following momentum equation normal to the shock:

$$\frac{u}{h_\xi}\frac{\partial v}{\partial \xi} + v\frac{\partial v}{\partial n} + u^2\left(\frac{h_{\xi s}}{h_\xi}\right)K_\xi + \frac{1}{\rho}\frac{\partial p}{\partial n} = 0 \tag{16}$$

Transforming this equation from the $\xi,\beta,n$ system to a new set of independent variables $\bar{\xi},\bar{\beta},\eta$ by using Eqs. (13) and (14) gives

$$\frac{\partial p}{\partial \eta} = \frac{\psi_s}{h_\beta}\left[\frac{1}{h_\xi}\frac{\partial v}{\partial \bar{\xi}} + u\left(\frac{h_{\xi s}}{h_\xi}\right)K_\xi\right] - \left(\frac{h_{\beta s}}{h_\beta}\right)\left(\frac{h_{\xi s}}{h_\xi}\right)\eta \sin\Gamma\frac{\partial v}{\partial \eta} \tag{17}$$

where

$$\bar{\xi} = \xi$$

$$\bar{\beta} = \beta$$

$$\eta = \psi/\psi_s$$

Note that $\eta = 1$ on the shock and $\eta = 0$ on the body surface. By substituting the coordinate $n$ into the transformation, an expression for the velocity component $v$ normal to the shock can be obtained and is given by

$$v = \frac{u}{h_\xi}\frac{\partial n}{\partial \bar{\xi}} + \left(\frac{h_{\beta s}}{h_\beta}\right)\left(\frac{h_{\xi s}}{h_\xi}\right)\frac{\eta \sin\Gamma}{\rho} \tag{18}$$

The only assumptions used in Eqs. (17) and (18) are that the velocity component $w = 0$ throughout the shock layer and that the curvilinear coordinate system is strictly orthogonal. However, to obtain explicit expressions for the pressure and normal velocity component, additional assumptions are required. The following approximations, which are consistent with the simplifications in Refs. 12 and 15, are valid for hypersonic flow and thin shock layers:

$$n \approx \left(\frac{\partial n}{\partial \eta}\right)_s (\eta - 1)$$

$$\frac{\partial \rho_s}{\partial \bar{\xi}} \approx 0$$

$$\frac{\partial v}{\partial \bar{\xi}} \approx 0$$

$$\rho \approx \rho_s$$

$$u \approx u_s$$

$$h_\xi \approx h_{\xi s}$$

$$h_\beta \approx h_{\beta s}$$

Equations (17) and (18) can now be simplified as

$$p(\bar{\xi},\bar{\beta},\eta) = p_s(\bar{\xi},\bar{\beta}) + \frac{\psi_s u_s K_\xi}{h_{\beta s}}(\eta - 1) - \frac{\psi_s v_s \tan\Gamma}{h_{\beta s}}(K_\xi + K_\beta)\frac{(\eta^2 - 1)}{2} \tag{19}$$

$$v(\bar{\xi},\bar{\beta},\eta) = v_s(\bar{\xi},\bar{\beta})\left[1 + \frac{\psi_s}{h_{\beta s}\cos\Gamma}(K_\xi + K_\beta)(\eta - 1)\right] \tag{20}$$

If $h_{\beta s} = r_s$, Eq. (19) becomes Maslen's second-order pressure equation for axisymmetric flow.[15] The pressure and normal component of velocity can now be found explicitly along a line normal to the shock surface since all variables in Eqs. (19) and (20) are evaluated on the shock. The surface pressure is found easily since the stream function $\psi$ and, thus, $\eta$ are zero on the body. Equations (19) and (20) are approximate.

*Other Relations*

The energy equation for steady, adiabatic, inviscid flow reduces to the simple relation that the total enthalpy of the flow is constant:

$$H = h + \tfrac{1}{2}(u^2 + v^2) = \text{const} \tag{21}$$

Also, for inviscid equilibrium or frozen flow, the (postshock) entropy is constant along a streamline. For a perfect gas, this may be expressed as

$$\left(\frac{p}{\rho^\gamma}\right)_{\psi,\beta} = \text{const} \tag{22}$$

With Eqs. (21) and (22), the density and streamwise component of velocity $u$ can be computed. The distance from the shock surface to the body along a line normal to the shock is calculated by integrating Eq. (13) and noting that the scale factor $h_\beta$ is a function of $n$ as given by Eq. (8). The distance $n_b$ is then given by

$$n_b - \frac{n_b^2 K_\beta}{2} = \frac{\psi_s}{h_{\beta s}}\int_0^1 \frac{d\eta}{\rho u} \tag{23}$$

Equations (19–23) for pressure, density, the two velocity components, and shock layer thickness outline an inverse method of solution in which the shock shape (not the body shape) is known. Therefore, the shock shape must be changed until the correct body shape is produced. The resulting iteration procedure is handled differently in each region of the flow.

**Method of Solution**

In the stagnation region of a blunt body traveling at hypersonic speeds, the flow is subsonic. Because of the elliptic behavior of the flowfield equations in this region, a marching scheme is not well posed. Thus, the complete shock shape for the entire subsonic-transonic region must be determined iteratively. A marching procedure is then used downstream of the subsonic-transonic region, where the flow is completely supersonic.

*Subsonic-Transonic Region*

In this investigation, the blunt-nose region of the body in a body-oriented coordinate system is represented by a longitudinal conic section with an elliptical cross section as

$$B_b y_b^2 + z_b^2 = 2R_b x_b - b_b x_b^2 \tag{24}$$

where $R_b$ is the nose radius of the body in the $x_b - z_b$ plane relative to the principal shock radius of curvature in the $x - z$ plane, $b_b$ determines the longitudinal shape of the body, and $B_b$ governs the ellipticity of the body cross section. This equation adequately describes the nose region of most re-entry vehicles. Van Dyke and Gordon[20] suggested that a conic-section body shape produces a shock surface that can also be described by a conic section. This assumption is used in the present analysis. Since a three-dimensional shock needs to be specified, longitudinal conic sections are blended in the circumferential direction by using one or more elliptical arcs to produce the shock surface in the subsonic region. One advantage to this approach is that parameters are added easily by blending more conic sections.

The equation of the longitudinal ($\phi$ = const) conic sections is given by

$$r_s^2 + b_i x_s^2 - 2c_i x_s + d_i x_s r_s = 0 \tag{25}$$

where $b_i$, $c_i$, and $d_i$ are parameters local to a plane where $\phi$ is constant in the wind-oriented system. At each $x$ location on the shock, the radii that are determined from Eq. (25) in each meridional plane are fitted with one or more elliptical segments to produce the circumferential variation of the shock radius. The number of parameters ($b_i$, $c_i$, and $d_i$) to calculate then depends on the number of planes. In this report, only three planes ($\phi = 0$, $\pi/2$, and $\pi$) are blended by using one cross-sectional ellipse to give a shock surface in the nose region. This method is adequate for axisymmetric shapes at angle of attack and for bodies with elliptical cross sections at moderate angles of attack. However, for elliptical bodies at larger angles of attack, more parameters and more elliptical segments may be needed to describe accurately the shock surface.

In the iteration procedure, the shock shape is first assumed to be equal to the body shape, and the conic-section parameters for the shock are chosen accordingly. Next, the shock standoff distance is computed from the limiting form of the shock layer equations on the stagnation line.[1] Shock lines are then traced from the stagnation region to the sonic surface by integrating the following differential equations that govern the shock shape along a shock line ($\beta$ = const):

$$\frac{\partial r_s}{\partial x} = \tan\Gamma \cos\delta_\phi \tag{26}$$

$$\frac{\partial \phi_s}{\partial x} = -\frac{\tan\Gamma \sin\delta_\phi}{r_s} \tag{27}$$

$$\frac{\partial \psi_s}{\partial x} = h_{\beta s} \tan\Gamma \tag{28}$$

$$\frac{\partial h_{\beta s}}{\partial x} = \tan\Gamma \frac{\partial \sigma}{\partial \beta} \tag{29}$$

$$\frac{\partial \sin\Gamma}{\partial x} = -K_\xi \tag{30}$$

where $x$ is the independent axial coordinate.[19] The shock variables are integrated along each shock line with a variable-step-size, third-order, predictor-corrector, ordinary differential equation solver. Angles and derivatives are determined by blending the longitudinal conic sections. Since these equations are indeterminate at the stagnation line ($x_s = 0$), the integration begins a small distance $\epsilon$ from the origin.[18] At $x_s = \epsilon$, the coordinate $\phi_s$ is assumed to be equal to the curvilinear coordinate $\beta$.

Equations (19–23) for pressure, density, velocity, and shock layer thickness are used to calculate the position of the body at each integration step. However, only a few of the calculated body points are constrained to match the actual body. These points are located primarily near the end of the subsonic-transonic region, where a good starting solution is crucial to the downstream marching procedure. The error between the geometric and calculated distance from the shock to the body is used to change the parameters of the shock surface in a quasi-Newton nonlinear equations solver. If the number of parameters is less than the number of calculated body points, the shock is determined in a least-squares sense. However, improved results downstream are obtained if the points on the body surface are matched exactly. Because three planes are used in this study, a total of nine parameters are varied until nine points on the body have the correct shock layer thickness.

*Supersonic Region*

Once past the transonic region, the flow is totally supersonic and a marching scheme is well posed. The shock surface and resulting shock lines from the transonic region form a starting solution for the marching procedure.

The differential equations that govern the shock shape along a shock line are given by Eqs. (26–30). However, in the supersonic region, $\delta_\phi$ and $\partial\sigma/\partial\beta$ are computed from finite differences in the circumferential direction at each $x$ location.

The general marching procedure is outlined here. Starting at $x_j$, predicted values for the shock variables ($r_s$, $\phi_s$, $\psi_s$, $h_{\beta s}$, $\sin\Gamma$) are obtained at $x_{j+1}$ for each shock line. The angle $\delta_\phi$ and the derivative $\partial\sigma/\partial\beta$ are computed using the predicted values of the shock radius. On each shock line, the local shock curvature $K_\xi$ is varied in Eqs. (19–23) until the calculated thickness matches the geometric shock layer thickness. Convergence usually requires two or three iterations with the secant method. These values of the shock curvature are now used to determine corrected values of the shock variables at $x_{j+1}$ for each shock line. Updated values for $\delta_\phi$, $\partial\sigma/\partial\beta$, and $K_\xi$ are calculated in the same fashion as in the predictor step. Upon completion of the corrector step at $x_{j+1}$ for each shock line, predicted values for the shock variables are obtained at $x_{j+2}$, and the entire process is repeated.

## Results and Discussion

Results at perfect-gas conditions are presented for this investigation over a paraboloid and an elliptic cone at angle of attack. Solutions are described in a body-oriented coordinate system with the circumferential angle $\phi_b = 0$ deg in the windward plane of symmetry and 180 deg along the leeward ray. Distances are referenced to the nose radius of the body. Nondimensional pressures are obtained by dividing by $\rho_\infty V_\infty^2$. Nineteen shock lines and 21 points along the $\eta$ direction are used for all solutions.

The present method is applicable for hypersonic Mach numbers ($M_\infty > 5$) and smooth nonaxisymmetric body shapes (i.e.,

no wings or fins). The approximations in the explicit pressure equation [Eq. (19)] improve as the freestream Mach number increases. Solutions at moderate angles of attack ($\alpha < \theta_c$) are presented here to avoid separation near the leeward plane. However, there appear to be no angle-of-attack limitations if only a solution near the windward plane is desired.

Shock shapes and surface pressures for a paraboloid at 12-deg angle of attack are presented in Figs. 3 and 4. Experimental results[21] are presented at freestream Mach numbers of 9.9 for the surface pressures and 5.73 for the shock shape. Although a paraboloid is axisymmetric, the shock shape produced in the nose region is fully three dimensional when the body is at angle of attack. Three longitudinal conic sections were blended by using a cross-sectional ellipse to produce the shock shape in the nose region. Six iterations using the quasi-Newton nonlinear equations solver were required for convergence. Good agreement (within 8%) in surface pressures between the present method and the experimental data[21] is shown in Fig. 3. In Fig. 4, the calculated shock lies slightly closer to the body than does the experimentally determined shock shape, but the agreement is good. Comparisons in Ref. 21 at 0-deg angle of attack were made with the axisymmetric Maslen technique of Zoby and Graves,[13] and a similar result was observed.

In order to demonstrate the ability of the present algorithm to calculate the flow about nonaxisymmetric body shapes,

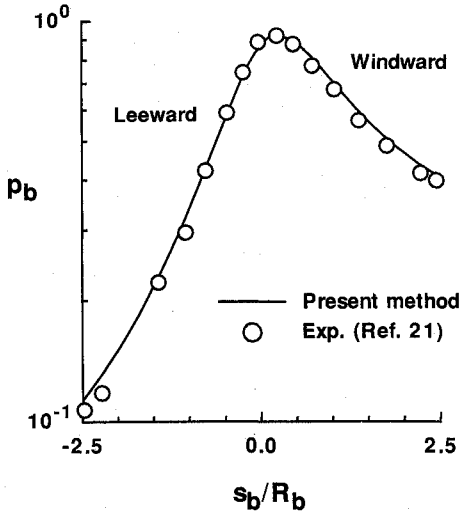


**Fig. 3 Axial surface pressure distribution in planes of symmetry on paraboloid with $\alpha = 12$ deg and $M_\infty = 9.9$.**

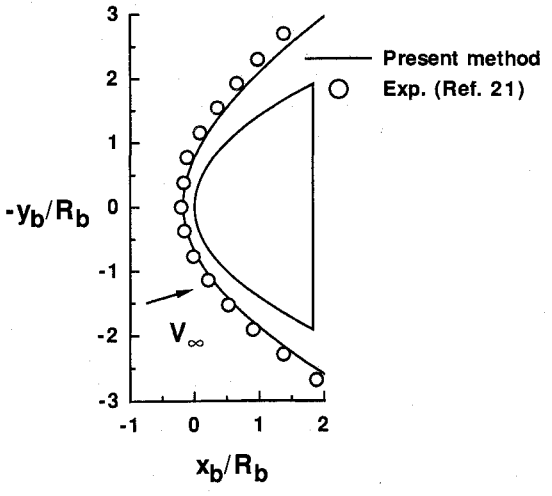


**Fig. 4 Shock shape in planes of symmetry for paraboloid with $\alpha = 12$ deg and $M_\infty = 5.73$.**

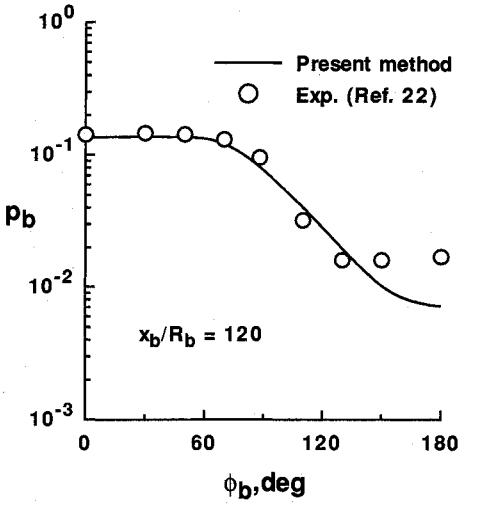


**Fig. 5 Circumferential surface pressure distribution on 1.5 elliptic cone with $\alpha = 10$ deg, $M_\infty = 10$, and $\theta_c = 10.26$ deg.**

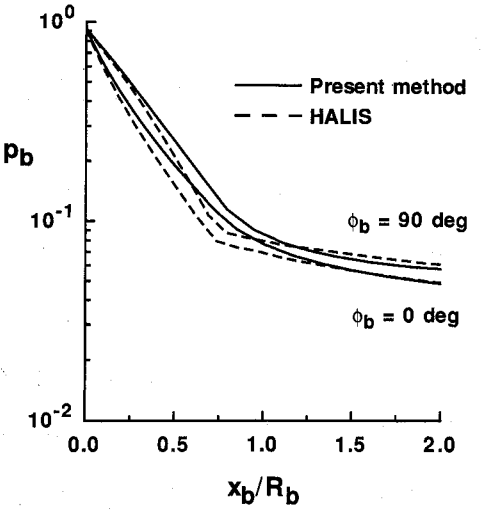


**Fig. 6 Axial surface pressure distribution on 1.5 elliptic nose with $\alpha = 0$ deg, $M_\infty = 10$, and $\theta_c = 10.26$ deg.**

surface pressures over an elliptic cone with a cone half-angle of 10.26 deg in the windward plane and an ellipticity of 1.5 are shown in Fig. 5. The experimental data[22] displayed are for a pointed elliptic cone. Since the present method currently allows for blunted bodies only, a very small bluntness is assumed for the elliptic cone. Circumferential pressures are shown for a position far downstream ($x_b/R_b = 120$), where the surface pressures should approach sharp cone values. At 10-deg angle of attack, the agreement between the experimental and calculated pressures is excellent except near the leeside region ($\phi_b > 140$ deg), as shown in Fig. 5. However, viscous effects are more pronounced in the leeward region, and an inviscid method is not appropriate for calculations in this area.

Solutions were also computed over a blunted elliptic cone with an ellipticity of 1.5 using two Euler equation solvers. The first, a time-dependent solution of the inviscid equations (HALIS),[4] is used to compute the blunt-nose region of the elliptic cone. The second Euler equation solver computes the supersonic region of the flow with a marching procedure (STEIN).[6] All three methods were run on a CRAY-2S supercomputer, and run times were compared. For a length of 2 nose radii, HALIS requires 1000 iterations for convergence and a time of 120 CPU s for a grid consisting of 31 points in the streamwise direction, 37 points in the circumferential direction, and 11 points in the shock layer. For the solution

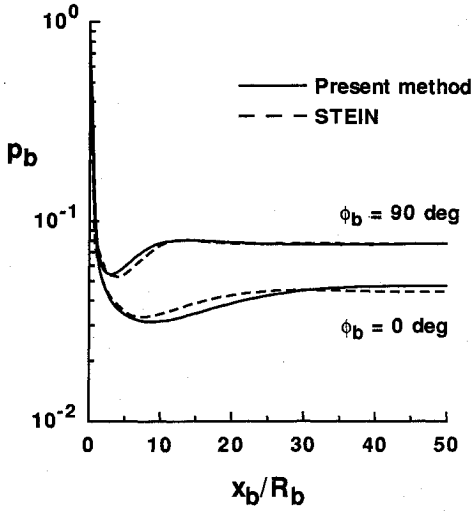


**Fig. 7 Axial surface pressure distribution on 1.5 elliptic cone with $\alpha = 0$ deg, $M_\infty = 10$, and $\theta_c = 10.26$ deg.**

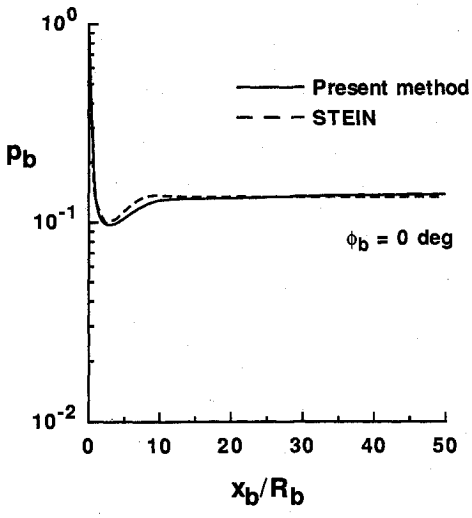


**Fig. 8 Axial surface pressure distribution on 1.5 elliptic cone with $\alpha = 10$ deg, $M_\infty = 10$, and $\theta_c = 10.26$ deg.**

downstream of the nose, STEIN requires 105 CPU s to advance 50 nose radii using 575 marching steps with a grid consisting of 37 points in the circumferential direction and 21 points in the shock layer. The present technique requires <1 CPU s to advance 50 nose radii using 65 marching steps, 19 points around the circumference of the shock, and 21 points in the shock layer. These comparisons indicate that the present technique is much faster than more exact CFD methods for three-dimensional nose shapes.

The surface pressure distribution in the planes of symmetry of the elliptic cone is shown in Figs. 6 and 7 for 0-deg angle of attack and a Mach number of 10. The surface pressure distribution in the windward plane of symmetry at 10-deg angle of attack is given in Fig. 8. The comparison in Ref. 19 of surface pressures on the elliptic cone is incorrect due to a misinterpretation of the HALIS results. The correct figure is shown here. For the comparisons presented in Fig. 6, the results from the present method are in good agreement with the more exact numerical solutions from HALIS, except near the nose-afterbody interface ($x_b/R_b \approx 0.75$). The same discrepancy has also been observed over axisymmetric shapes. The streamwise derivative of the normal velocity component, which is assumed to be equal to zero in the explicit pressure equation [Eq. (19)], is not negligible in this region. This error is a result of the assumptions used to obtain Maslen's axisymmetric method and is not caused by the three-dimensional modifications. However, excellent agreement is obtained farther downstream with results from the present method and the STEIN solution, as shown in Figs. 7 and 8. Circumferential pressure distributions in the nose region and on the conical afterbody are given in Figs. 9 and 10 for the elliptic cone at 0- and 10-deg angles of attack. Good agreement is noted except on the leeward side ($\phi_b > 90$ deg) of the elliptic cone at angle of attack. Thus, the errors due to the approximations used in the explicit pressure equation [Eq. (19)] appear to be limited to the nose-afterbody interface region.

Radial profiles of pressure and density on the blunted nose and on the conical afterbody are depicted in Figs. 11 and 12 in the windward symmetry plane. Note that the profiles are normalized with respect to the shock position given by the Euler solvers, HALIS and STEIN. The properties from the present method agree well (within 10%) with the more exact numerical results. Engineering aerodynamic heating methods require not only accurate surface properties but also accurate properties in the shock layer in order to correctly account for entropy-layer swallowing. The present method would be a good choice to provide these engineering aerodynamic heating methods with both surface and shock layer properties.

Note that, although aerodynamic information important to preliminary studies can be obtained with the present three-dimensional method, a significant application of the method is

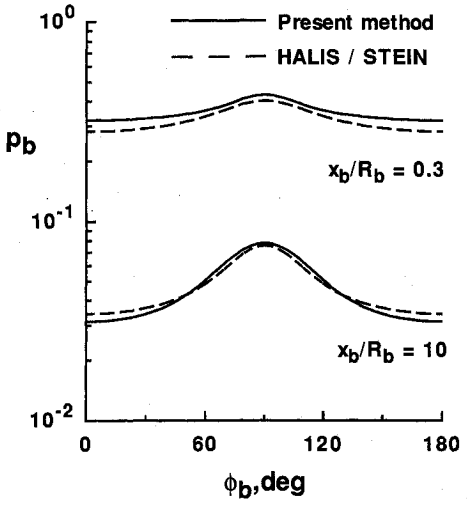


**Fig. 9 Circumferential surface pressure distribution on 1.5 elliptic cone with $\alpha = 0$ deg, $M_\infty = 10$, and $\theta_c = 10.26$ deg.**

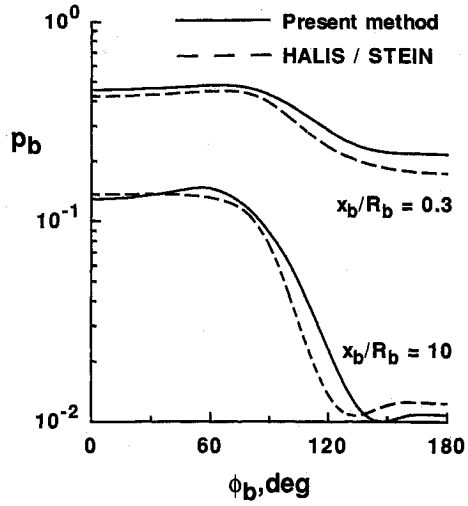


**Fig. 10 Circumferential surface pressure distribution on 1.5 elliptic cone with $\alpha = 10$ deg, $M_\infty = 10$, and $\theta_c = 10.26$ deg.**

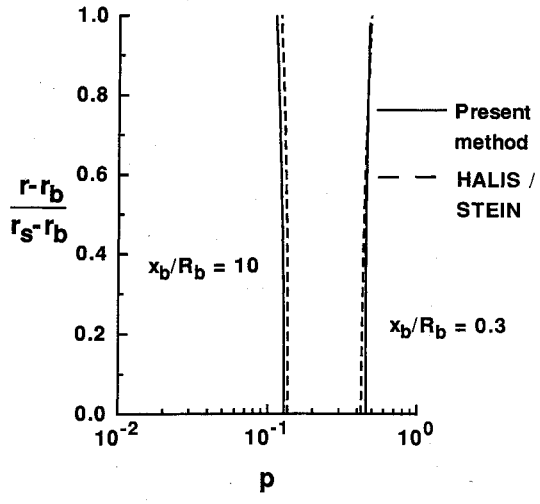


**Fig. 11 Radial profile of pressure in windward symmetry plane on 1.5 elliptic cone with $\alpha = 10$ deg, $M_\infty = 10$, and $\theta_c = 10.26$ deg.**

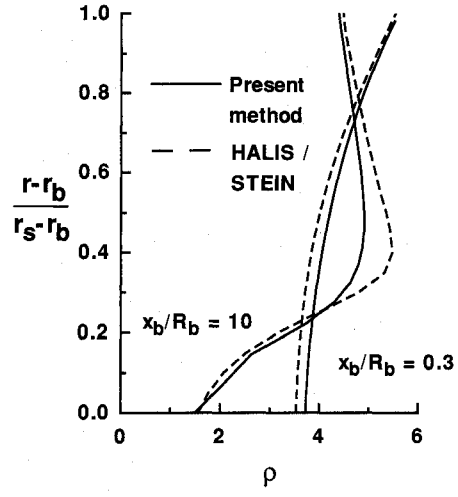


**Fig. 12 Radial profile of density in windward symmetry plane on 1.5 elliptic cone with $\alpha = 10$ deg, $M_\infty = 10$, and $\theta_c = 10.26$ deg.**

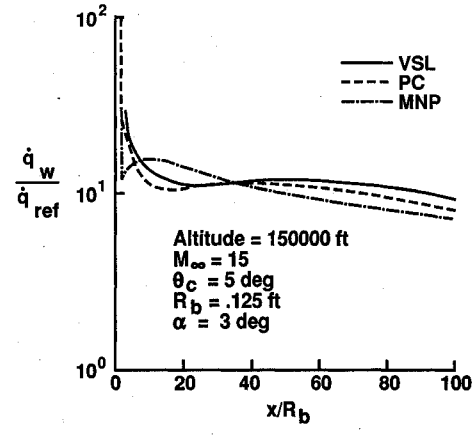


**Fig. 13 Influence of pressure distribution on surface heating rates in windward symmetry plane on spherically blunted cone with $\alpha = 3$ deg (from Ref. 23).**

the calculation of heating rates over the vehicles. The importance of obtaining good flowfield and surface pressures for predicting surface heating rates was demonstrated in Ref. 23. An accurate pressure correlation and modified Newtonian pressures were used to compute properties and values of the local metric for an approximate heating method, and the results along the windward ray were compared with results of a detailed code (VSL). The comparison (taken from Ref. 23) is presented here as Fig. 13 for a blunted 5-deg cone at 3-deg angle of attack. The agreement of approximate and detailed heating rates is significantly improved when the more accurate pressure correlation is used.

## Concluding Remarks

An approximate technique has been developed that determines the flowfield over blunt-nose bodies at hypersonic speeds. An explicit expression from Maslen for the pressure across the shock layer and the assumption of approximate stream surfaces in the shock layer are used to simplify the three-dimensional flow. The method is applied to the solution over a paraboloid and an elliptic cone at angle of attack for a perfect gas.

The present technique predicts shock surfaces and shock layer properties that are in good agreement with the more exact numerical solutions and experimental results. The method is very rapid when compared with the more exact finite difference solutions of the inviscid equations, in particular, the solution over bodies with three-dimensional noses. Therefore, this technique should be especially attractive for engineering aerodynamic heating methods that require inviscid hypersonic flowfield information.

## References

[1]DeJarnette, F. R., and Hamilton, H. H., "Aerodynamic Heating on 3-D Bodies Including the Effects of Entropy-Layer Swallowing," *Journal of Spacecraft and Rockets,* Vol. 12, No. 1, 1975, pp. 5–12.

[2]Zoby, E. V., and Simmonds, A. L., "Engineering Flowfield Method with Angle-of-Attack Applications," *Journal of Spacecraft and Rockets,* Vol. 22, No. 4, 1985, pp. 398–405.

[3]Hamilton, H. H., DeJarnette, F. R., and Weilmuenster, K. J., "Application of Axisymmetric Analog for Calculating Heating in Three-Dimensional Flows," *Journal of Spacecraft and Rockets,* Vol. 24, No. 4, 1987, pp. 296–302.

[4]Weilmuenster, K. J., and Hamilton, H. H., "Calculations of Inviscid Flow over Shuttle-Like Vehicles at High Angles of Attack and Comparisons with Experimental Data," NASA TP-2103, May 1983.

[5]Weilmuenster, K. J., Smith, R. A., and Greene, F. A., "Assured Crew Return Vehicle Flowfield and Aerodynamic Characteristics," AIAA Paper 90-0229, Jan. 1990.

[6]Marconi, F., Salas, M., and Yaeger, L., "Development of a Computer Code for Calculating the Steady Super/Hypersonic Inviscid Flow Around Real Configurations. Volume I—Computational Technique," NASA CR-2675, April 1976.

[7]Morrison, A. M., Solomon, J. M., Ciment, M., and Ferguson, R. E., "Handbook of Inviscid Sphere-Cone Flow Fields and Pressure Distributions: Volume I," Naval Surface Weapons Center, NSWC/WOL/TR 75-45, Silver Spring, MD, Dec. 1975.

[8]Gnoffo, P. A., "An Upwind-Biased, Point-Implicit Relaxation Algorithm for Viscous, Compressible Perfect-Gas Flows," NASA TP-2953, Feb. 1990.

[9]Lawrence, S. L., Chaussee, D. S., and Tannehill, J. C., "Application of an Upwind Algorithm to the Three-Dimensional Parabolized Navier-Stokes Equations," AIAA Paper 87-1112, June 1987.

[10]Thompson, R. A., "Comparison of Nonequilibrium Viscous-Shock-Layer Solutions with Shuttle Heating Measurements," *Journal of Thermophysics and Heat Transfer,* Vol. 4, No. 2, 1990, pp. 162–169.

[11]Swaminathann, S., Kim, M. D., and Lewis, C. H., "Three-Dimensional Nonequilibrium Viscous Shock-Layer Flows over Complex Geometries," AIAA Paper 83-0212, Jan. 1983.

[12]Maslen, S. H., "Inviscid Hypersonic Flow Past Smooth Symmetric Bodies," *AIAA Journal,* Vol. 2, No. 6, 1964, pp. 1055–1061.

[13]Zoby, E. V., and Graves, R. A., Jr., "A Computer Program for Calculating the Perfect Gas Inviscid Flow Field About Blunt Axisymmetric Bodies at an Angle of Attack of 0 Deg," NASA TM X-2843, Dec. 1973.

[14]Jackson, S. K., Jr., "The Viscous-Inviscid Hypersonic Flow of a Perfect Gas over Smooth Symmetric Bodies," Ph.D. Dissertation, Univ. of Colorado, Boulder, CO, Aug. 1966.

[15]Maslen, S. H., "Asymmetric Hypersonic Flow," NASA CR-2123, Sept. 1972.

[16]Maslen, S. H., "Development of a Method of Analysis and Computer Program for Calculating the Inviscid Flow About the

Windward Surfaces of Space Shuttle Configurations at Large Angles of Attack," NASA CR-132453, Jan. 1974.

[17]Maslen, S. H., "Inviscid Flow About Blunted Cones of Large Opening Angle at Angle of Attack," NASA CR-132652, March 1975.

[18]DeJarnette, F. R., and Hamilton, H. H., "Inviscid Surface Streamlines and Heat Transfer on Shuttle-Type Configurations," *Journal of Spacecraft and Rockets,* Vol. 10, No. 3, 1973, pp. 314-321.

[19]Riley, C. J., and DeJarnette, F. R., "An Approximate Method for Calculating Three-Dimensional Inviscid Hypersonic Flow Fields," NASA TP-3018, Aug. 1990.

[20]Van Dyke, M. D., and Gordon, H. D., "Supersonic Flow Past a Family of Blunt Axisymmetric Bodies," NASA TR R-1, 1959.

[21]Miller, C. G., III, "Measured Pressure Distributions, Aerodynamic Coefficients, and Shock Shapes on Blunt Bodies at Incidence in Hypersonic Air and CF4," NASA TM-84489, Sept. 1982.

[22]Palko, R. L., and Ray, A. D., "Pressure Distribution and Flow Visualization Tests of a 1.5 Elliptic Cone at Mach 10," Arnold Engineering Development Center, AEDC-TDR 63-163, Arnold AFB, TN, Aug. 1963.

[23]Riley, C. J., DeJarnette, F. R., and Zoby, E. V., "Surface Pressure and Streamline Effects on Laminar Heating Calculations," *Journal of Spacecraft and Rockets,* Vol. 27, No. 1, 1990, pp. 9-14.

Ernest V. Zoby
*Associate Editor*